Sinop Üniversitesi Fen Bilimleri Dergisi *Sinop Uni J Nat Sci 4 (1): 1-20(2019)*
ISSN: 2536-4383

Research Article **https://doi.org/10.33484/sinopfbd.315643**

Green Synthesis and Characterization of CuO Nanoparticles: Telon Blue AGLF and Methylene Blue Adsorption

Bayram ÇİMEN, Sonya ŞENGÜL, Memduha ERGÜT*, Ayla ÖZER

Mersin University, Faculty of Engineering, Department of Chemical Engineering, 33343 Yenişehir, Mersin, Turkey.

Abstract

In this study, CuO nanoparticles (CuO NPs) were synthesized using *Acacia cyanophylla* leaves aqueous extract as a non-toxic, easily available and cost-effective reducing agent. The green synthesized CuO NPs were characterized by SEM/EDX, DLS, FT-IR and XRD analysis. Subsequently, Telon Blue AGLF (TB AGLF) and Methylene Blue (MB) adsorption onto the CuO NPs were carried out and optimum adsorption conditions were investigated. Optimum conditions were determined as initial pH 7 and 8, temperature 25°C and adsorbent concentration 1 g/L for TB AGLF and MB, respectively. Also; a linear increase was observed in adsorbed dye amounts with increasing both initial dye concentrations. Furthermore, CuO NPs were also synthesized by chemical reduction method to investigate the effect of synthesis method of CuO NPs on the adsorptions of both dyes. The results showed that, higher adsorption capacities were obtained in the experiments which were conducted by green synthesized CuO NPs than chemically synthesized. Experimental equilibrium data were better fitted to the Langmuir and Freundlich isotherm models for TB AGLF and MB, respectively. The calculated free energy values from D-R isotherm model, were lower than 8 kJ/mol which was indicating that the both adsorption processes proceeded through physisorption. The adsorption kinetics of TB AGLF and MB onto CuO NPs showed the better suitability of pseudo-second-order kinetic model; and, Weber-Morris intraparticle diffusion model showed that, not only intraparticle both also film diffusion resistances were influential in the adsorption processes.

Keywords: *Acacia cyanophylla,* CuO nanoparticle, Adsorption, Methylene Blue, Telon Blue AGLF

CuO Nanopartiküllerinin Yeşil Sentezi ve Karakterizasyonu: Telon Blue AGLF ve Metilen Mavisi Adsorpsiyonu

Öz

Bu çalışmada; toksik olmayan, kolay elde edilebilir ve ucuz bir indirgeyici ajan olarak Kıbrıs akasyası yaprağı sulu özütü ile bakır oksit (CuO) nanopartikülleri sentezlenmiştir. Yeşil sentezlenen nanopartiküllerin, SEM/EDX, DLS, FT-IR ve XRD analiz yöntemleri ile karakterizasyonu gerçekleştirilmiştir. Ardından Telon Blue AGLF (TB AGLF) ve Metilen Mavisinin (MB) CuO NPs'ye adsorpsiyonu gerçekleştirilmiş ve optimum adsorption koşulları incelenmiştir. TB AGLF ve Metilen Mavisinin adsorpsiyonu için optimum ortam koşulları sırasıyla, pH 7 ve 8, sıcaklık 25°C, ve adsorbent derişimi 1 g/L olarak belirlenmiştir. Ayrıca; her iki boyarmadde için, başlangıç boyarmadde derişimlerinin artması ile dengede adsorplanan boyarmadde miktarlarının doğrusal olarak arttığı gözlenmiştir. Ek olarak, her iki

* Corresponding Author: ORCID ID: orcid.org/ 0000-0001-7297-1533
e-mail: memduha.ergut@gmail.com
Received: 24.05.2017
Accepted: 06.01.2019

boyarmaddenin adsorpsiyonu üzerinde CuO NPs sentez yönteminin etkisinin araştırılması amacıyla, CuO NPs kimyasal indirgeme yöntemi ile de sentezlenmiştir. Sonuçlar, yeşil sentezlenmiş CuO NPs ile yürütülen deneysel çalışmalarda, kimyasal indirgeme yöntemi kullanılarak sentezlenmiş nanopartiküllere göre, daha yüksek adsorpsiyon kapasitelerinin elde edildiğini göstermiştir.
Adsorpsiyon denge verilerinin TB AGLF ve MB için sırasıyla Langmuir ve Freundlich modellerine daha iyi uyduğu belirlenmiştir. Dubinin–Radushkevich izoterm modelinden hesaplanan adsorpsiyon serbest enerjilerinin ise 8 kJ/mol'den daha düşük olması, her iki boyarmaddenin adsorpsiyonunun fiziksel olarak gerçekleştiğini göstermiştir. TB AGLF ve MB'nin CuO NPs'ye adsorpsiyon kinetiğinin yalancı ikinci mertebe kinetik modele daha uygun olduğu belirlenmiş ve ayrıca Weber - Morris tanecik içi difüzyon modeli, her iki adsorpsiyonda iç difüzyonun yanısıra dış difüzyon dirençlerinin de etkili olduğunu göstermiştir.

Anahtar kelimeler: *Acacia cyanophylla,* CuO nanopartikül, Adsorpsiyon, Metilen Mavisi, Telon Blue AGLF

Introduction

In the recent years, using metal oxide nanoparticles as adsorbents have been receiving special attention because of their great specific surface area and porous nature for removal of synthetic dyestuffs from aqueous solutions by adsorption.

Copper oxide (CuO) is a significant industrial material for wide variety applications such as heterogeneous catalysis, electrode material, gas sensors, magnetic storage media, semiconductors, solar cells, solar energy transformation, reactive oxidizers in nanothermite composites; owing to its small band gap (1.21–1.51 eV) [1]. Moreover, CuO has emerged as a potential adsorbent material for the removal of contaminants from wastewaters and it has been extensively used as an environmental catalyst [2]. Dashamiri et al. reported that; Copper oxide nanoparticles loaded on activated carbon (CuO NPs-AC) were a novel adsorbent for rapid, sensitive and high capacity simultaneous ultrasound-assisted adsorption of brilliant green (BG), auramine O (AO), methylene blue (MB) and eosin yellow (EY) dyes [3]. Sharma et al. studied the catalytic thermal decomposition of ammonium perchlorate (AP) using green CuO NPs as the heterogeneous catalyst [1].

Conventionally various methods such as; precipitation/co-precipitation, thermal decomposition, sol-gel, laser ablation, sonochemical reaction, microwave radiation, alcothermal, hydrothermal process and electrochemical methods etc. have used for the preparing of CuO nanoparticles. These chemical synthesis methods are very efficient, however; they are suffer from many limitations such as, being costly, using expensive, flammable organic solvents and toxic chemicals, formation of toxic by-

products. So, they do not fulfill the necessities of eco- friendly chemical processes [4]. Therefore; to overcome these disadvantages, nowadays; there is a growing attention in development of facile, green and alternative synthesis procedures with minimized environmental impact. The biosynthetic techniques for the synthesis of metal oxide nanoparticles by exploitation from microorganisms, enzyme and plant/plant extracts provide cost effective, low energy, pressure and temperature conditions also, they do not involve hazardous chemicals.

Among these biosynthetic methods, the using of plant extracts as a reducing or capping agents has several advancements such as easily available, safe to handle, use of non-toxic solvents like water, simplicity and suitability for scale-up steps of preparation of metal oxide nanoparticles.

Acacia cyanophylla is one of the flowering plants of *Fabaceae* family located in mainly Australia, hot temperate and semi-tropical regions. It was recorded that *A. cyanophylla* has high level of proanthocyanidins (condensed tannins) which are phenolic seconder metabolites may be responsible for bioreduction of metallic ions and preparing the metal oxide nanoparticles [5].

In this this study, CuO NPs were biosynthesized by using *A. cyanophylla* leaves aqueous extract and characterised. The synthesized CuO NPs were used as an adsorbent for the removal of anionic and cationic dyes.

Materials and Methods

Chemicals

All the chemicals used in experiments were of analytical grade and was used without further purification. $CuSO_4.5H_2O$ in synthesis of nanoparticle was obtained from Carlo Erba. Telon Blue AGLF was supplied by Dye Star and Methylene Blue was purchased from Merck.

Green synthesis of CuO nanoparticles

Acacia cyanophylla leaves were collected from Mersin, Turkey. Aqueous extract of *A. cyanophylla* leaves was prepared by heating the certain amount of dried leaves in 100°C at 500 mL of distilled water for 1 h. The filtered extract was mixed with an equal volume of 0.01 mol/L $CuSO_4.5H_2O$ solution and the final mixture was stirred vigorously at 130 °C for 7 h. After 30 min, it was observed that, the color of solution began to change from green to dark brown during the heating process which indicates the formation of CuO nanoparticles. The dark brown solid product was washed with distilled water after being separated from the suspension by centrifugation and then, dried in oven at

120°C for 8 h [6]. The dried mass was further annealed at 600°C for 4 h in a furnace in order to achieve highly crystalline and stable nanoparticles.

Moreover, in order to investigate the effect of synthesis method of CuO NPs on the adsorption of TB AGLF and MB dyes, the CuO NPs were synthesized by chemical reduction method with NaOH solution instead of *A. cyanophylla* leaves aqueous extract as a reducing agent. For the chemical synthesis of CuO NPs, 0.01 mol/L $CuSO_4.5H_2O$ solution was prepared and then, the pH value of the solution was adjusted to 12 by adding 0.1 M sodium hydroxide solution. After that, the solution was stirred for around 30 min to allow the reaction to complete. The color change of the solution from green to black indicated a successful chemical reduction reaction.

Then, the obtained nanoparticles were washed with distilled water after being separated from the suspension by centrifugation and dried in oven at 120°C for 8 h. The dried nanoparticles were further calcined at 600°C for 4 h.

Characterization of CuO nanoparticles

The functional groups of the CuO NPs before and after adsorption were determined by Fourier transform infrared spectrometer (FT-IR) analysis carried out in the range of 4000–400 cm^{-1}. XRD analysis was performed, using nickel-filtered Cu Kα radiation in a Philips XPert MPD apparatus operated at 40 kV and 30 mA, in the 2θ range of 10°–80° to explain the crystal structure of CuO NPs. The morphology of the adsorbent was analyzed by Zeiss/Supra 55 SEM analysis and Zeiss/Supra 55 energy dispersive X-ray analyzer (EDX) was used to obtain elemental and quantitative composition of CuO NPs. DLS analysis was performed in a Malvern Zetasizer Nano ZS to determine the average particle size of synthesized CuO NPs.

Batch adsorption studies

The adsorption experiments were conducted in 250 mL Erlenmayer flasks containing 100 mL of adsorption solution. The initial pHs of each dye solutions were adjusted with 0.1 M HCl and 0.1 M NaOH solutions before adding adsorbent. 0.1 g of CuO NPs, except for adsorbent concentration experiments, was mixed with 100 mL of dye solution at known initial dye concentration and initial pH in an Erlenmayer flask. Then the flasks were agitated on a shaker at a constant temperature for 180 min to reach adsorption equilibrium. Samples were taken before adding the CuO NPs and dye bearing solution and at pre-determined time intervals for the residual dye concentration in the solution. Then, samples were

centrifuged at 3500 rpm for 5 min and the supernatant liquid was analyzed. The unadsorbed TB AGLF and MB dye concentration were determined at 610 and 662 nm wavelength with spectrophotometer, respectively. Experiments were repeated for different initial pH, initial dye concentration, temperature and adsorbent concentration values. The adsorbed dye amount [q_e (mg/g)] and the percentage of adsorption (%) at equilibrium were calculated as follows:

$$q_e = (C_o - C_e)/X_o \quad (1)$$

$$\text{Adsorption (\%)} = ((C_o - C_e)/ C_o) \times 100) \quad (2)$$

where, the initial and equilibrium dye concentration (mg/L), are symbolized by C_o and C_e respectively, and the adsorbent concentration in solution (g/L) is X_o.

Results and Discussion

Characterization of CuO NPs

In this study, the particle size and size distribution of the green synthesized CuO NPs were determined with DLS equipment. Moreover, the average particle size has been estimated by Williamson-Hall equation using XRD data of the CuO NPs after calcination and Image J program using SEM images. The mean hydrodynamic radius of the CuO NPs was measured to be 169.6 ± 3.56 nm by DLS analysis. Particle size distribution of the synthesized CuO NPs by DLS analysis was presented in Figure 1 and Table 1.

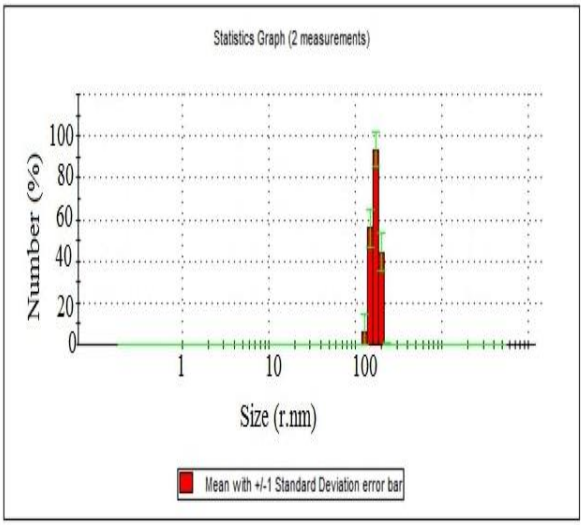

Figure 1. *Particle size distribution of green synthesized CuO NPs*

Table 1. *Particle size distribution values of green synthesized CuO nanoparticles*

Size r.nm	Mean number %	Std Number %
127.5	3.00	4.3
147.7	27.9	4.6
171.0	46.8	4.0
198.0	22.1	4.6
229.3	0.20	0.3

The average particle size of CuO NPs was calculated to be 77.57 nm by using Image J program using randomly selected 150 particles from SEM images.

Using the modified form of Williamson–Hall method, we have calculated particle size D through the following equation [7]:

$$\beta\cos(\theta) = k\lambda/D + 4\varepsilon\sin(\theta) \quad (3)$$

where 'β' is FWHM (full width at half maximum), 'θ' is the diffraction angle, 'λ' is wave length of X-Ray (0.1541 nm), Ɛ is strain and 'D' is particle diameter size. The strain and particle size are calculated from the slope and y-intercept (kλ/D) of Williamson–Hall plot, i.e. the plot of between 4sin(θ) and βcos(θ). The slope of graph gives strain and the intercept on the axis gives the particle size corresponding to zero strain [7, 8]. The average particle size of CuO NPs was calculated as 69.3 nm by using Williamson–Hall method. The particle size of the CuO NPs estimated from the SEM images were a little larger than that obtained from XRD data.

This signify that, the SEM images indicates the size of polycrystalline particles since, no surfactant was used in this study. Therefore, CuO NPs had the tendency to agglomerate because of high surface tension of the ultrafine nanoparticles [9]. The determination of the largest particle size of CuO NPs by DLS analysis maybe attributed to the fact that, DLS measurements suffered from absorption effects and particle scattering because of agglomeration [10].

SEM images of green synthesized CuO NPs were presented in Figure 2. a,b,c before and after adsorption. As seen from SEM images of pre-adsorption (Figure 2-a), the synthesized CuO NPs have the spherical morphology, nano-sized and porous structure. The SEM images of CuO NPs after TB AGLF and MB dyes adsorption are shown in Figure 2-b and c. According to post-adsorption SEM images, an increase was observed in particle size of CuO NPs due to adsorption of TB AGLF anions and MB cations onto the CuO NPs surface.

EDX analysis results given in Table 2. The results showed that, the elemental and quantitative weight composition (wt.%) of synthesized CuO NPs were composed of 45.7% Cu, 18.4% O, 30.7% C, 2.64% S and 2.5% N elements. The elemental compositions were determined as 29.64% Cu, 25.5% O, 38.67% C, 4% N, 2.02% S and 0.79% Na after TB AGLF adsorption; and 32% Cu, 25.75% O, 35.73% C, 4.72% N, 1.2% S and 0.6% Cl after MB adsorption. EDX analysis results revealed high Cu and O elements content; also, the presence of C, O, S and N elements derived from aqueous leaf extract. Moreover, the presence of Na and Cl elements results from adsorption of dye molecules onto CuO NPs.

ISSN: 2536-4383

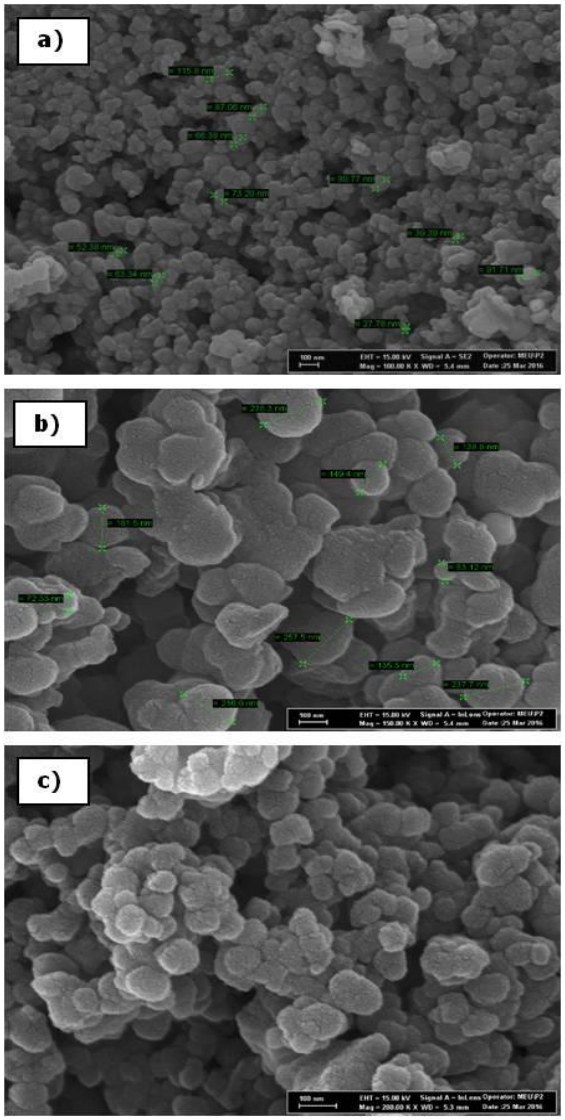

Figure 2. *SEM images (a) pre-adsorption (b) After TB AGLF adsorption (c) after MB adsorption*

Table 2. *EDX elemental analysis results for pre- and post- adsorption*

Element	Weight (%)		
	Green synthesized CuO NPs pre-adsorption)	CuO NPs after TB AGLF adsorption	CuO NPs after MB adsorption
Cu	45.70	29.64	32.00
O	18.40	25.50	25.75
C	30.70	38.67	35.73
S	2.640	4.000	4.720
N	2.500	2.020	1.120
Na	-	0.790	-
Cl	-	-	0.600

The green synthesized CuO NPs which wrere examined by XRD analysis, displayed the amorphous structure before calcination (figure not shown). The XRD pattern of the CuO NPs after calcination was shown in Figure 3.

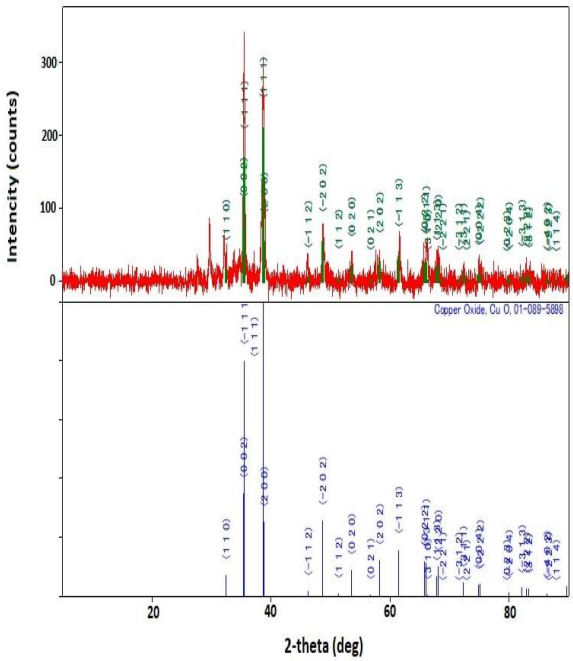

Figure 3. *XRD patterns of gren synthesized CuO NPs*

ISSN: 2536-4383

High crystalline of CuO NPs were obtained after calcination at 600°C for 4h. The observed diffraction peaks are well indexed with the corresponding planes of copper oxide. According to XRD pattern, the nanoparticles had typical monoclinic structure of CuO NPs without any other phases. The XRD peaks were obtained at (0,0,2); (1,1,0); (1,1,1); (1,1,-2), (2,0,0); (2,0,-2); (0,2,0); (2,0,2); (1,1,-3); (0,2,2), (1,1,3) and (0,0,4) Bragg's reflection based on the crystalline nature of CuO NPs [11]. XRD patterns of CuO NPs before and after adsorption were presented in Figure 4.

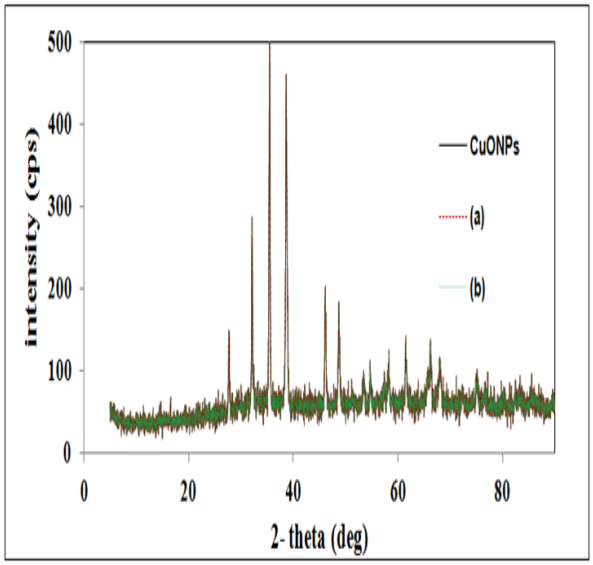

Figure 4. *XRD patterns of CuO NPs before and after adsorption (a)TB AGLF (b) MB*

According to Figure 4, no significant differences were observed in XRD patterns of CuO NPs before and after adsorption. This case revealed that, crystallinity and phase of the CuO NPs did not changed in adsorption.

FT-IR spectrums of *A. cyanophylla* leaves crude extract and green synthesized CuO NPs, were presented in Figure 5-a and b, respectively.

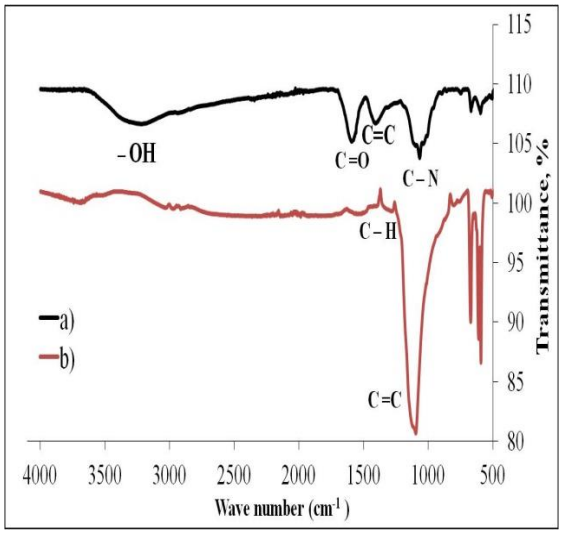

Figure 5. *FT-IR spectrum of (a) crude extract and (b) green synthesized CuO NPs*

According to Figure 5-a, the broad peak at 3226.56 cm^{-1} could be attributed to the stretching vibration of adsorbed moisture and surface hydroxyl group related to the phenolic compounds. The bands observed at 1595.14 cm^{-1}, 1407.22 cm^{-1}, 1283.71 cm^{-1} and 1068.10 cm^{-1} represent C=O carbonyl group stretching C=C aromatic ring, C-H or C-O stretching vibrations and stretching vibrations of C-N functional groups of amines, respectively. These peaks show the presence of phenolic compounds in the plant extract. The

phenolic compounds in the *A. cyanophylla* leaves extract may be responsible for formation of nanoparticles by bioreducing of metal ions.

The FT-IR spectra of synthesized CuO NPs (Figure 5-b) depicted the peaks at 1097.54 cm^{-1} and 1283.71 cm^{-1} which represent C-O (polyols) and C-H or C-O stretching vibrations of methyl, methoxy and methylene groups. Especially, the bands ranging 1000–1300 cm^{-1} originate most probably from the C-O group of hydroxyflavones and other phenolics in the *A. cyanophylla* leaves extract [12]. The IR bands at 460 cm^{-1}, 594 cm^{-1} and 612 cm^{-1} correspond to the stretching vibration of Cu–O bond in monoclinic CuO and the peak observed at 805 cm^{-1} correspond to C – O vibrations in CuO [1, 6, 13]. These peaks proved that, CuO NPs were synthesized successfully.

FT-IR spectrums of CuO NPs after TB AGLF adsorption and MB adsorption were presented in Figure 6-a and b, respectively. As seen from FT-IR spectrums given in Figure 6, no significant structural changes were observed between dye-unloaded and dye-loaded CuO NPs. FT-IR analysis results indicated that, the adsorption of TB AGLF and MB onto CuO NPs was proceeded physically since, any bond formation or breaking was not detected after adsorption. This case supported the XRD results in terms of any difference did not observed in crystal structure of CuO NPs pre-and post-adsorption.

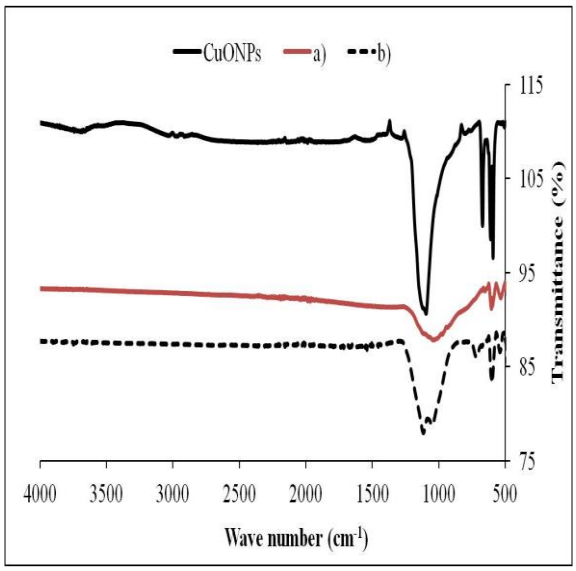

Figure 6. *FT-IR spectrums of CuO NPs after adsorption for (a) TB AGLF (b) MB*

Effect of Optimum Environmental Conditions

The effect of initial pH

The influence of initial pH on TB AGLF and MB adsorption onto CuO NPs was given Figure 7.

As seen from Figure 7, the optimum initial pH values were determined as 7.0 and 8.0 for TB AGLF and MB, respectively. The initial pH affected the adsorption capacity of CuO NPs by interaction between dye molecules and the surface charges of adsorbent [14].

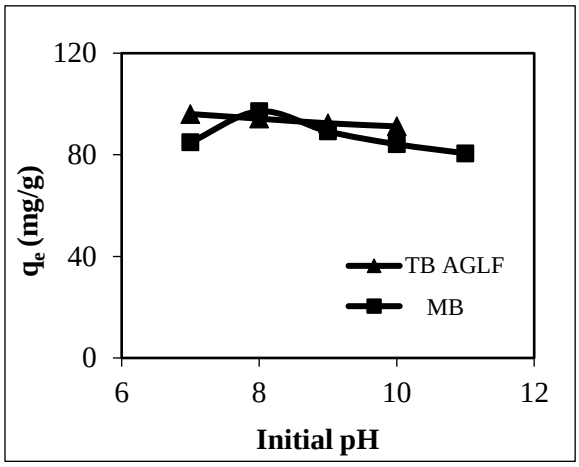

Figure 7. *Effect of initial pH (Co= 100 mg/L, Xo= 1g/L, T=25°C, t= 180 min)*

The net surface charges of CuO NPs were determined by measuring ζ (zeta) potential at different pH values and the change of ζ potential with pH was presented in Figure 8. As seen from Figure 8, it was observed that the CuO NPs surface was negatively charged all pH values and had maximum negative charge at pH 8.0 value (-23.76 mV). At this pH, the adsorbed MB amount was maximum due to strong electrostatic attractions between MB dye cations and negatively charged surface. However, if the adsorbent surface is negatively charged, the electrostatic attraction/repulsion theory, did not fully describe the removal of anionic TB AGLF dye at basic pH. This case might be explained with ion exchange mechanism [15], between negatively charges surface and Na^+ ions in TB AGLF dye structure. A comparable tendency was obtained for the adsorption of an anionic dye, eosin Y from aqueous solution by chitosan hydrobeads.

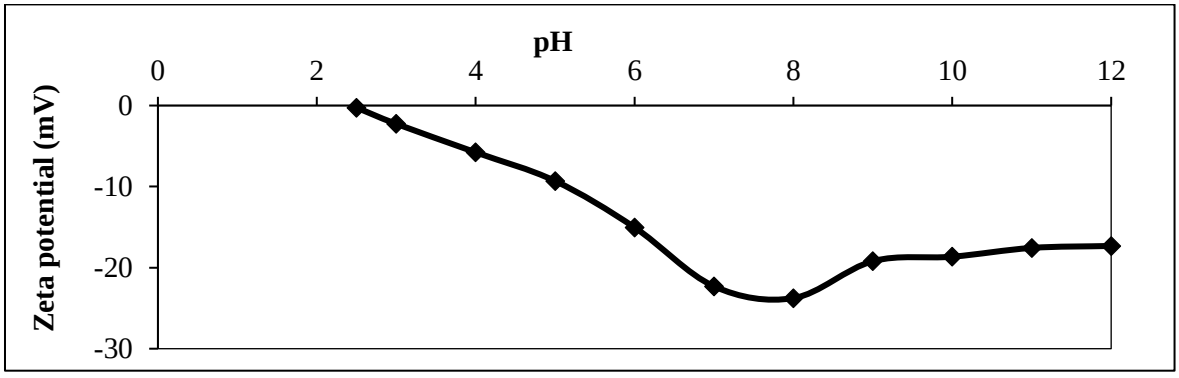

Figure 8: *Variation of ζ potential with pH for CuO NPs*

Researchers indicated that the maximum sorption capacity of the chitosan hydrobeads remained practically unchanged from pH 4.0 up to pH 8.0 and beyond this range a sharp decrease was noted [16]. In this work; at pH 7.0, the removal of TB AGLF was maximum as a consequence of high ionic attraction (-22.3 mV) and ζ potential values were approximately same, after pH 9.0.

Effect of initial dye concentration

The plot of the equilibrium uptakes (mg dye /g adsorbent) of TB AGLF and MB onto CuO NPs vs. the initial dye concentrations was depicted in Figure 9.

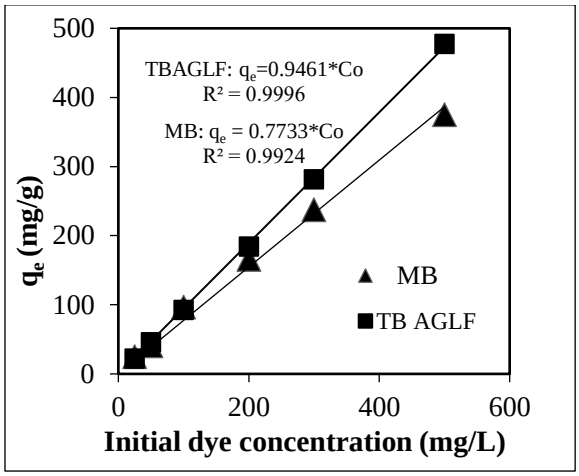

Figure 9. *Effect of initial dye concentration (pH 7.0 and 8.0 for TB AGLF and MB, Xo= 1g/L, T=25°C, t=180 min)*

As seen from Figure 9, the equilibrium uptakes of TB AGLF and MB by the CuO NPs were enhanced linearly in accordance with $q_e=0.9461*C_o$ ($R^2=0.9996$) and $q_e=0.7733*C_o$ ($R^2=0.9924$) equations, respectively. It was observed that, the adsorbed dye amounts at equilibrium increased by increasing initial dye concentration at constant adsorbent concentration as a result of increasing the driving force the concentration gradient (ΔC), to get over mass transfer resistances of the dyes between the aqueous and solid phases. The structures of the adsorbent and adsorbed material cause selectivity in adsorption. It was seen from Figure 9, TB AGLF was higher adsorbed selectively in adsorption.

Effect of temperature

The temperature effect on the TB AGLF and MB adsorption by CuO NPs was presented in Figure 10. As seen from Figure 10, higher adsorption capacities obtained in lower temperatures as a result of the exothermic characters of the adsorption processes. Consequently, the optimum adsorption temperature for the studied dyes was determined as 25°C. Furthermore, the adsorbed dye amounts were higher at lower temperatures. This was indicated that both dyes were bound to active sites of the CuO NPs physically.

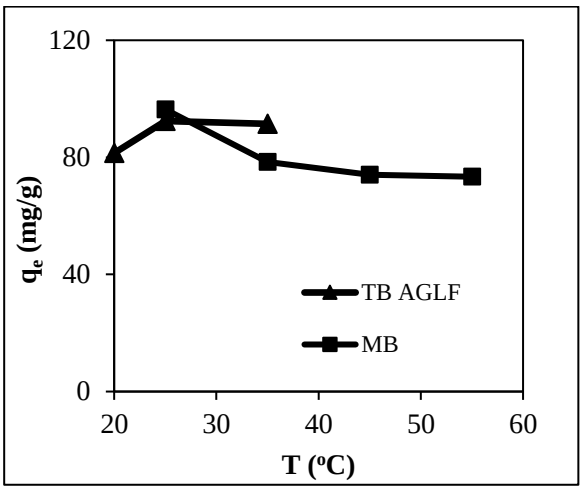

Figure 10. *Effect of temperature (Co= 100 mg/L, pH 7.0 and 8.0 for TB AGLF and MB, Xo= 1g/L)*

Effect of adsorbent concentration

The effect of adsorbent concentration on adsorption of TB AGLF and MB by CuO NPs was investigated in the range of 0.5–3.0 g/L adsorbent concentration and the variation of equilibrium uptake values and adsorption percentages with adsorbent concentration were shown in Figure 11.

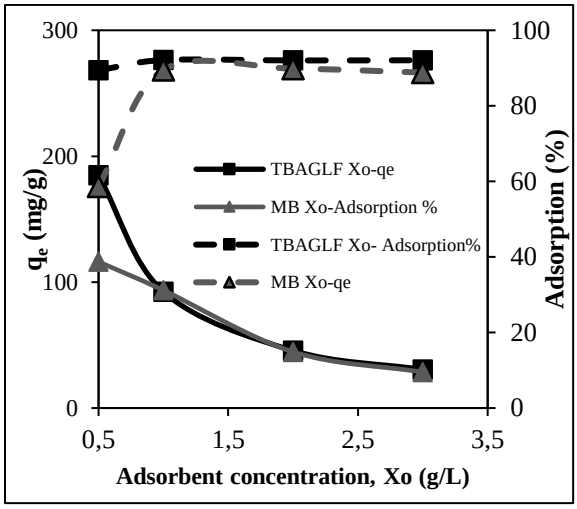

Figure 11. *Effect of adsorbent concentration (Co= 100 mg/L, pH 7.0 and 8.0 for TB AGLF and MB, T= 25°C, t=180 min)*

According to Figure 11, it was observed that, when the adsorbent concentration was increased, the adsorbed TB AGLF and MB amounts per unit mass of adsorbent decreased but, percent of removals increased. This was ascribed to an increase in accessible surface area and adsorption sites that notably enhanced by the increasing the amount of adsorbent [17]. On the other hand, the agglomeration of adsorbent particles at higher concentrations, which would give rise to a decrease in the active surface area of adsorbent and an increase in the diffusional path length for this reason, the adsorbed dye amounts per unit mass of adsorbent (q_e; mg/g) decreased. Hereby, the optimum adsorbent concentration was chosen as 1.0 g/L for TB AGLF and MB adsorption.

Effect of synthesis method of CuO NPs on the adsorptions

The effect of synthesis method of CuO NPs on the adsorption of TB AGLF and MB dyes was presented in Figure 12. The adsorption studies were performed at the optimum environmental conditions for both dyes.

As seen from Figure 12, the significantly lower q_e values were obtained with chemically synthesized CuO NPs compared to green synthesized CuO NPs. This case could be due to improving of the adsorbent properties of CuO NPs by the contribution of many special functional groups which were came from *A. cyanophylla* leaves aqueous extract on the CuO NPs stucture. The presense of functional groups in the structure of CuO NPs were indicated in the FT-IR spectrum (Figure 5(b)).

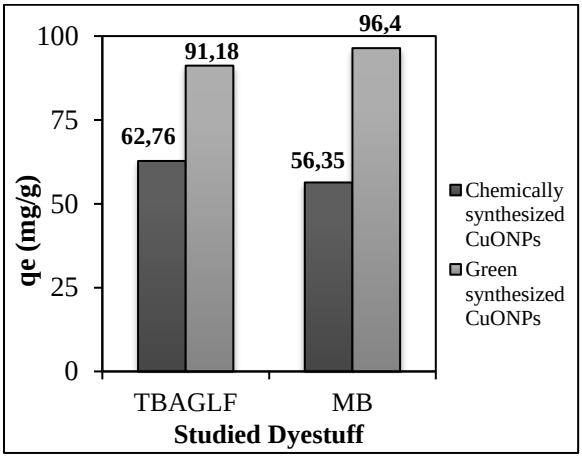

Figure 12. *Effect of synthesized method of CuO NPs on the adsorption (Co=100 mg/L, pH 7.0 and 8.0 for TB AGLF and MB, T= 25°C, Xo= 1 g/L, t=180 min)*

Equilibrium, Kinetic and Mass Transfer Modelling

In this study, to describe the adsorption behaviors of TB AGLF and MB onto CuO NPs, the linear forms of the Langmuir [$1/q_e=1/Q^ob(1/C_e)+1/Q^o$], Freundlich [$\ln q_e=\ln K_F+(1/n)\ln C_e$] and Dubinin–Radushkevich [$\ln q_e= \ln q_m-\beta.\varepsilon^2$] isotherm models were implemented to the experimental equilibrium data obtained at 25°C and 35°C temperatures. The isotherm constants with regression coefficients (R^2) are presented in Table 3.

According to Table 3, the adsorption equilibrium for TB AGLF and MB best defined the Langmuir isotherm model and Freundlich isotherm model, respectively. Therefore, this results demonstrated that, the TB AGLF adsorption occured at specific homogeneous sites within the adsorbent forming monolayer coverage of dye at the surface of CuO NPs, while MB adsorption take place on the heterogeneous adsorption sites on the surface of CuO NPs.

Also, it was observed from Table 3, the maximum adsorption capacities obtained from isotherm models were at 25°C, which was the optimum operation temperature for both dye adsorption.

Table 3. *The isotherm model constants and regression coefficients.*

	T	Langmuir			Freundlich			D-R		
	(°C)	Q^o	b	R^2	K_F	1/n	R^2	q_m	E	R^2
TB AGLF	25	476.19	0.0424	0.996	1.424	1.3725	0.973	614.65	50.00	0.930
	35	412.19	0.0199	0.997	1.232	1.4119	0.987	470.78	70.71	0.973
MB	25	285.71	0.0146	0.992	5.968	0.755	0.999	204.54	50.00	0.947
	35	84.746	0.0278	0.946	5.672	0.504	0.997	90.04	35.35	0.975

The comparison of dye adsorption capacities of CuO NPs and CuO NPs composite materials in the literature was given in Table 4. According to Table 4, green synthesized CuO NPs using *A. cyanophylla* leaves extract used in this

study showed higher maximum monolayer adsorption capacity for TB AGLF dye than others. This could be expressed by significant structural differences of the adsorbents due to variety of the synthesis methods and differences of the dyes.

Referring to the K_F; Freundlich isotherm constant value, the adsorption capacity of CuO NPs for MB adsorption was higher than that of some studies in the literature as seen from Table 5. The obtaining high values of K_F was also indicated that CuO NPs had high adsorption capacity and affinity for MB molecules

Table 4. *The comparison of the monolayer coverage capacities of CuO NPs for dyes*

Adsorbent	Synthesis Method	Dye	Q°(mg/g)	Reference
CuO NPs loaded on activated carbon (CuO-NP-AC)	CuO NPs: Sol-gel	Methylene Blue	9.72	[17]
CuO embedded chitosan spheres	CuO NPs: Precipitation with NaOH	Methyl orange	28.2	[18]
CuO/Al_2O_3 catalyst	Incipient wetness impregnation	Reactive Black 5	91.2	[19]
CuO NPs loaded on activated carbon (CuO NPs-AC)	CuO NPs: Precipitation with NH_4OH	Brilliant green (BG), Auramine O (AO), Methylene Blue (MB) Eosin yellow (EY)	BG: 94.93 AO: 94.66 MB: 97.58 EY: 96.22	[3]
Synthetic zeolite NaA/CuO	Ion-exchange	Methyl orange	79.49	[20]
CuO NPs	Biosynthesis using *A. cyanophylla* leaves extract	Telon Blue AGLF Methylene Blue	TB AGLF: 476.19 MB: 285.71	This study

ISSN: 2536-4383

Table 5. *The comparison of adsorption capacities referring to Freundlich isotherm constant value (K_F) for MB adsorption.*

Adsorbent	Dye	K_F	Reference
Graphite	Methylene Blue	0.893	[21]
Multi-walled carbon nanotubes (MWCNTs) decorated with $CoFe_2O_4$ nanoparticles	Methylene Blue	1.598	[22]
Mesostructured silica nanoparticles (MSNAP)	Methylene Blue	3.330	[23]
Oak sawdust composite	Methylene Blue	3.442	[24]
CuO NPs	Methylene Blue	5.968	This study

Dubinin–Radushkevich isotherm model (D–R) was applied to interpret whether the dye adsorption mechanisms were physisorption or chemisorption. The linear form of the D–R isotherm equation is stated as follows:

$$\ln q_e = \ln q_m - \beta.\varepsilon^2 \quad (4)$$

where q_m is the maximum adsorption capacity (mg/g), ε is the Polanyi potential [$\varepsilon = RT \ln(1+1/C_e)$] and β is the activity coefficient associated to adsorption mean free energy. The values of q_m and β are obtained from the intercept, and slope by plotting ln q_e versus ε^2, respectively. The adsorption mean free energy was calculated from following equation:

$$E = 1/(\sqrt{2\beta}) \quad (5)$$

The E value gives idea about adsorption mechanism is chemical or physical adsorption. If the magnitude of E is between 8 and 16 kJ/mol, the adsorption is controlled by a chemical mechanism, while for E < 8 kJ/mol, the adsorption follows a physical mechanism [25, 26]. The free energy values determined from D-R isotherm model, were lower than 8 kJ/mol which was showed that the TB AGLF and MB adsorptions proceeded through physical mechanism.

The linear forms of the pseudo-first-order ($\log(q_e - q_t) = \log(q_e) - k_1 t/2.303$) and pseudo-second-order ($(t/q_t) = (1/q_e^2 k_2) + (t/q_e)$) kinetic models were applied to the kinetic data and the model constants with regression coefficients were presented in Table 6.

Table 6. *The kinetic and intraparticle model constants with regression coefficients*

Co (mg/L)		$q_{e,exp}$	Pseudo-first-order			Pseudo-second-order			Weber-Morris model		
			$k_1 x10^3$	$q_{e,cal1}$	R^2	k_2 $x10^3$	$q_{e,cal2}$	R^2	K_i	I	R^2
TB AGLF	50	45.592	15.4	36.626	0.914	1.281	41.633	0.972	4.194	0.107	0.997
	100	92.401	18.2	75.457	0.938	0.625	84.289	0.965	8.923	0.626	0.997
	200	184.19	30.6	112.69	0.976	0.975	184.19	0.995	14.50	58.81	0.993
	300	281.45	26.7	106.34	0.747	1.317	281.45	0.999	15.60	119.1	0.990
	500	477.20	21.9	129.03	0.650	1.575	477.20	0.999	24.75	324.8	0.970
MB	50	40.287	11.3	17.758	0.644	9.185	40.287	0.998	10.76	1.092	0.996
	100	96.402	15.8	76.700	0.979	0.818	96.402	0.985	10.86	2.444	0.977
	200	165.46	8.75	148.08	0.935	0.524	165.46	0.974	10.89	37.06	0.965
	300	237.41	6.45	228.50	0.759	0.607	228.59	0.996	28.17	37.07	0.979
	500	401.44	8.06	383.88	0.898	0.245	379.98	0.982	32.81	58.04	0.996

As seen from Table 6, when the regression coefficients and the experimental and calculated q_e values were compared, both dye adsorption kinetics were in the best agreement with the pseudo-second-order kinetic model.

Weber–Morris intraparticle diffusion model was used to determine the effect of the film and intraparticle diffusions on adsorptions. The equation of the Weber–Morris model is as follows:

$$q_e = K_i .t^{0.5} + I \quad (6)$$

where K_i, is the intra-particle diffusion rate constant, which was evaluated from the slope of the linear plot of q_e versus $t^{0.5}$. The value of I, gives the information about thickness of the boundary layer and it was determined from the intercept [17].

According to equation, if the intraparticle diffusion model is effective in adsorption process, the plot of q_e vs. $t^{0.5}$ should be linear and pass through the origin. Conversely, the slope will be linear but will not pass through the origin when an initial film mass transfer is predominated [25]. The plot is multilinear when both intraparticle and film diffusion are influential on the adsorption. In this study, as seen from Table 6, both intraparticle and film diffusions played an effective role on the adsorptions of TB AGLF and MB onto CuO NPs.

Conclusions

In the present work, CuO NPs were biosynthesized by using *A. cyanophylla* leaves aqueous extract. Then FT-IR, SEM, EDX, XRD, and DLS analysis techniques were used for the characterization of nanoparticles. DLS analysis results showed that, the hydrodynamic radius of particles as to be 169.6 ± 3.56 nm due to quite agglomeration tendency of nanoparticles. But, the average particle size of CuO NPs was calculated to be 77.57 nm according to Image J program using randomly selected

150 particles from SEM images and, the average particle size of CuO NPs was found as 69.3 nm by using Williamson–Hall method. SEM images revealed that CuO NPs were synthesized successfully with a diameter nano- sized as well as spherical and porous. According to EDX analysis, the CuO NPs were mainly consist of the elements of Cu, O, and C. Additionaly FT-IR and XRD results supported the CuO NPs were synthesized successfully.

Afterwards, the adsorptions of TB AGLF and MB onto CuO NPs were investigated in a batch mode and the results were given as follows:

The optimum adsorption conditions for TB AGLF and MB adsorption onto CuO NPs were determined as initial pH values 7.0 for TB AGLF and 8.0 for MB, temperature 25°C and adsorbent concentration 1.0 g/L. The adsorbed TB AGLF and MB amounts at equilibrium increased linearly with increasing the initial dye concentration for the studied dyes. The adsorption equilibrium data best fitted to Langmuir isotherm model for TB AGLF adsorption and Freundlich isotherm model for MB adsoprtion. The maximum monolayer adsorption capacity was obtained as 476.19 mg/g for TB AGLF dye and Freundlich isotherm constant value was found to be 5.968 $(mg/g(L/g)^{1/n})$ for MB adsorption at optimum temperature value of 25°C. Moreover, the free energy values determined from D-R isotherm model were lower than 8 kJ/mol. Therefore TB AGLF and MB adsorptions proceeded through physical mechanism.

The kinetic and mass transfer models were evaluated in order to determine the adsorption mechanism and the results showed that, the kinetic data were well-fitted with the pseudo-second-order kinetic model for both dyes adsorption, and both intraparticle diffusion and external mass transfer were effective according to Weber-Morris model for both dye adsorrptions onto CuO NPs.

The effect of synthesis method of CuO NPs on the adsorptions of both two dyes were investigated by green synthesized and chemically synthesized CuO NPs. As a result, higher adsorption capacities were obtained in the adsorption experiments which were conducted by green synthesized CuO NPs than chemically synthesized.

Consequently, the green synthesized CuO NPs by *A. cyanophylla* leaves aqueous extract without using any chemical agents, could be effective adsorbent for TB AGLF and MB removal from aqueous solutions.

Nomenclature

b : A constant related to the affinity of the binding sites (L/mg)

C_e : Unadsorbed dye concentration at equilibrium (mg/L)
C_o : Initial dye concentration (mg/L)
E : Adsorption energy (J/mole)
K_F : Freundlich constant indicating adsorption capacity ((mg/g)/(L/mg)$^{1/n}$)
K_i : Intraparticle diffusion rate constant (mg/g.min$^{0.5}$)
k_1 : Pseudo first order kinetic rate constant (1/min)
k_2 :Pseudo second order kinetic rate constant (g/mg.min)
q_e :Adsorbed amount per unit mass of adsorbent (mg/g)
q_m :Maximum adsorption capacity obtained from D-R isotherm model (mg/ g)
q_{e,cal_1} :Calculated adsorbed amount per unit mass of adsorbent from pseudo first order kinetic model (mg/g)
q_{e,cal_2} :Calculated adsorbed amount per unit mass of adsorbent from pseudo second order kinetic model (mg/g)
$q_{e,exp}$:Experimental adsorbed amount per unit mass of adsorbent (mg/g)
q_t :Adsorbed amount per unit mass of adsorbent at any time (mg/g)
Q^o :Maximum monolayer coverage capacity of adsorbent (mg/g)
1/n : Freundlich constant indicating adsorption intensity

References

[1] Sharma JK, Srivastava P, Singh G, Akhtar MS, Ameen S, 2015. Catalytic thermal decomposition of ammonium perchlorate and combustion of composite solid propellants over green synthesized CuO nanoparticles. Thermochimica Acta, 614: 110-115.

[2] Verma M, Gupta VK, Dave V, Chandra R, and Prasad GK, 2015. Synthesis of sputter deposited CuO nanoparticles and their use for decontamination of 2-chloroethyl ethyl sulfide (CEES). Journal of Colloid and Interface Science, 438: 102-109.

[3] Dashamiri S, Ghaedi M, Dashtian K, Rahimi MR, Goudarzi A, Jannesar R, 2016. Ultrasonic enhancement of the simultaneous removal of quaternary toxic organic dyes by CuO nanoparticles loaded on activated carbon: central composite design, kinetic and isotherm study. Ultrasonics Sonochemistry, 31: 546-557.

[4] Nasrollahzadeh M, Maham M, Sajadi SM, 2015. Green synthesis of CuO nanoparticles by aqueous extract of Gundelia tournefortii and evaluation of their catalytic activity for the synthesis of N-monosubstituted ureas and reduction of 4-nitrophenol. Journal of Colloid and Interface Science, 455: 245-253.

[5] Reed JD, Soller H, and Woodward A, 2015. Fodder tree and straw diets for sheep: intake, growth, digestibility and the effects of phenolics on nitrogen utilisation. Animal Feed Science and Technology, 30(1): 39-50.

[6] Gunalan S, Sivaraj R, Venckatesh R, 2012. Aloe barbadensis Miller mediated green synthesis of mono-disperse copper oxide nanoparticles: optical properties. Spectrochimica Acta Part A: Molecular and Biomolecular Spectroscopy, 97:1140-1144.

[7] Prabhu YT, Rao KV, Kumar VSS, Kumari BS, 2014. X-ray analysis by Williamson-Hall and size-strain plot methods of ZnO nanoparticles with fuel variation. World Journal of Nano Science

and Engineering, 4(01): 21.

[8] Singh V, Chauhan P, 2009. Structural and optical characterization of CdS nanoparticles prepared by chemical precipitation method. Journal of Physics and Chemistry of Solids, 70(7):1074-1079.

[9] Theivasanthi T, Alagar M, 2009. X-ray diffraction studies of copper nanopowder. arXiv preprint arXiv, 1003.6068.

[10] Heller A, Fleys MS, Chen J, van der Laan GP, Rausch MH, Fröba AP, 2016. Thermal and Mutual Diffusivity of Binary Mixtures of n-Dodecane and n-Tetracontane with Carbon Monoxide, Hydrogen, and Water from Dynamic Light Scattering (DLS). Journal of Chemical & Engineering Data, 61(3):1333-1340.

[11] Nasrollahzadeh M, Sajadi SM, Rostami-Vartooni A, 2015. Green synthesis of CuO nanoparticles by aqueous extract of Anthemis nobilis flowers and their catalytic activity for the A^3 coupling reaction. Journal of Colloid and Interface Science, 459:183-188.

[12] Nasrollahzadeh M, Sajadi SM, 2016. Pd nanoparticles synthesized in situ with the use of Euphorbia granulate leaf extract: Catalytic properties of the resulting particles. Journal of Colloid and Interface Science, 462:243-251.

[13] Sharmila G, Thirumarimurugan M, Sivakumar VM, 2016. Optical, catalytic and antibacterial properties of phytofabricated CuO nanoparticles using Tecoma castanifolia leaf extract. Optik-International Journal for Light and Electron Optics, 127(19): 7822-7828.

[14] Aksu Z, Tatlı Aİ, Tunç Ö, 2008. A comparative adsorption/biosorption study of Acid Blue 161: Effect of temperature on equilibrium and kinetic parameters. Chemical Engineering Journal, 142(1): 23-39.

[15] Namasivayam C, Prabha D, Kumutha M, 1998. Removal of direct red and acid brilliant blue by adsorption on to banana pith. Bioresource Technology, 64(1): 77-79.

[16] Chatterjee S, Chatterjee S, Chatterjee BP, Das AR, Guha AK, 2005. Adsorption of a model anionic dye, eosin Y, from aqueous solution by chitosan hydrobeads. Journal of Colloid and Interface Science, 288(1):30-35.

[17] Ghaedi M, Ghaedi AM, Hossainpour M, Ansari A, Habibi MH, Asghari AR, 2014. Least square-support vector (LS-SVM) method for modeling of methylene blue dye adsorption using copper oxide loaded on activated carbon: Kinetic and isotherm study. Journal of Industrial and Engineering Chemistry, 20(4): 1641-1649.

[18] Khan SB, Ali F, Kamal T, Anwar Y, Asiri AM, Seo J, 2016. CuO embedded chitosan spheres as antibacterial adsorbent for dyes. International Journal of Biological Macromolecules, 88:113-119.

[19] Bradu C, Frunza L, Mihalche N, Avramescu, SM, Neaţă M, Udrea I, 2010. Removal of Reactive Black 5 azo dye from aqueous solutions by catalytic oxidation using CuO/Al_2O_3 and NiO/Al_2O_3. Applied Catalysis B: Environmental, 96(3):548-556.

[20] Mekatel EH, Amokrane S, Aid A, Nibou D, Trari M, 2015. Adsorption of methyl orange on nanoparticles of a synthetic zeolite NaA/CuO. Comptes Rendus Chimie, 18(3), 336-344.

[21] Yan, H., Tao, X., Yang, Z., Li, K.,

Yang, H., Li, A., Cheng, R, 2014 Effects of the oxidation degree of graphene oxide on the adsorption of methylene blue. Journal of hazardous materials, 268, 191-198.

[22] Farghali, AA, Bahgat M, El Rouby WMA, Khedr MH, 2012. Decoration of MWCNTs with $CoFe_2O_4$ nanoparticles for methylene blue dye adsorption. Journal of Solution Chemistry, 41(12): 2209-2225.

[23] Karim AH, Jalil AA, Triwahyono S, Sidik SM, Kamarudin NHN, Jusoh R, Hameed BH, 2012. Amino modified mesostructured silica nanoparticles for efficient adsorption of methylene blue. Journal of colloid and interface science, 386(1): 307-314.

[24] El-Latif, MA, Ibrahim AM, El-Kady MF, 2010. Adsorption equilibrium, kinetics and thermodynamics of methylene blue from aqueous solutions using biopolymer oak sawdust composite. Journal of American Science, 6 (6):267-283.

[25] Uzunoğlu D, Özer A, 2016. Adsorption of Acid Blue 121 dye on fish (Dicentrarchus labrax) scales, the extracted from fish scales and commercial hydroxyapatite: equilibrium, kinetic, thermodynamic, and characterization studies. Desalination and Water Treatment. 57(30): 14109-14131.

[26] Özcan A, Öncü EM, Özcan AS, 2006. Kinetics, isotherm and thermodynamic studies of adsorption of Acid Blue 193 from aqueous solutions onto natural sepiolite. Colloids and Surfaces A:Physicochemical and Engineering Aspects, 277(1): 90-97.